*minerals*

MDPI

*Article*

# Process Mineralogy of Li-Enriched Pegmatite Combining Laboratory Mineral Separations and SEM-Based Automated Image Analysis

**Marco Timich, Renato Contessotto and Carina Ulsen ***

Technological Characterization Laboratory (LCT-USP), Mining and Petroleum Department, Universidade de São Paulo, Av. Prof. Mello Moraes, 2373, São Paulo 05588-030, SP, Brazil
* Correspondence: carina.ulsen@usp.br

**Abstract:** Brazil has 95 million tons of Li reserves in the form of pegmatites but produces less than 1% of the global output. Historically Li production in Brazil has been low due to governmental restrictions aimed at controlling the exploitation and trade of Li in Brazil. However, as of 2022, these restrictions were revoked. The abundance of untapped pegmatite ores in Brazil complements the soaring demand for Li in energy-storage applications. This study performs process mineralogy studies on 10 samples collected from a Li pegmatite deposit in the southeastern region of Minas Gerais in Brazil. The samples were characterized by combining density separation and SEM-based automated mineralogy processing system allied with XRF, ICP OES, XRD, and LA–ICPMS. The latter was used to determine Li content in micas which allowed determining the Li deportment between Li-bearing minerals. The results show that the samples contain such Li-bearing minerals as muscovite (0.5 wt% $Li_2O$) and lepidolite (3.1 wt% $Li_2O$), in addition to spodumene (8.0 wt% $Li_2O$). According to the characterization of the spodumene concentrate (d = 3.11) by density separation (at d = 2.95), two main trends were observed: (a) low Li deportment in the sink product (approximately 44% wt%) and higher $Li_2O$ grade (approximately 6.5 wt%), and (b) higher Li deportment in the sink product (58%) and lower $Li_2O$ content (approximately 4.9 wt%). The first trend is associated with higher modal content of mica since it carries Li to the light product. Lower Li grade is related to the presence of Fe-bearing minerals (e.g., epidote and amphibole) as they report to the dense product and do not contain Li. Spodumene has a high degree of liberation in all samples; therefore, it did not influence the deportment results. The findings highlight the benefit of combining scanning electron microscopy-based automated mineralogy with LA–ICPMS and other techniques from process mineralogy studies in mineral processing. In addition to the mineralogy and liberation characteristics, identifying Li-bearing minerals and determining Li deportment is crucial.

**Keywords:** automated mineralogy; spodumene; Li; LA–ICPMS



**Citation:** Timich, M.; Contessotto, R.; Ulsen, C. Process Mineralogy of Li-Enriched Pegmatite Combining Laboratory Mineral Separations and SEM-Based Automated Image Analysis. *Minerals* **2023**, *13*, 343. https://doi.org/10.3390/min13030343

Academic Editor: Dianwen Liu

Received: 22 January 2023
Revised: 23 February 2023
Accepted: 24 February 2023
Published: 28 February 2023



## 1. Introduction

Demand for Li has surged owing to its applicability in green energy-storage technologies [1]. To cater to this demand, metallurgists require an extensive knowledge of its uses and sources to maximize the use of mineral concentrates [2]. In Brazil the main Li source are pegmatites, and, currently, reserves account for 1% of the global Li reserve. However, recent studies reveal a promising scenario where this share may increase significantly [3].

Pegmatites are igneous rocks that possess a distinct, extremely coarse texture with a variable grain size and a mostly granitic composition [4]. Pegmatites are divided into two "families" by chemical composition: those containing Nb, Y, and F (NYF family) and those containing Li, Cs, and Ta (LCT Family). The latter is the main source of Li [5].

LCT pegmatites typically contain 12–30% spodumene, 22–27% quartz, 30–50% feldspar, 3–5% mica, and other accessory minerals, including cassiterite and columbite [1]. Spodumene ($LiAlSi_2O_6$, 8.0% $Li_2O$), a Li–Al silicate, is the most common Li-containing ore

mineral [6]. However, Li can also be found in many different minerals, such as petalite ($LiAlSi_4O_{10}$, 4.89% $Li_2O$), lepidolite ($K(Li,Al)_3(Si,Al)_4O_{10}(F,OH)_2$, 5.9% $Li_2O$), zinnwaldite ($KLiFeAl(AlSi_3)O_{10}(F,OH)_2$, 4.14% $Li_2O$), and amblygonite ($(Li,Na)Al(PO_4)(F,OH)$, 10.1% $Li_2O$) [7]. Potential by-products to Li in pegmatites can be mainly Sn, Ta, Nb, and Be.

Currently, Greenbushes Lithium Operations in Western Australia is one of the largest producers of Li worldwide [8]. Its reserve is hosted in pegmatite and is estimated to be over 30 million tons, with at least 7 million tons at 4.0% $Li_2O$ [9]. Other known pegmatite-processing plants worldwide include Mt. Cattlin, Mt. Marion, and Bald Hill in Australia, Mibra in Brazil, Bernic Lake in Canada, Bikita in Zimbabwe, and Kings Mountain in the US [10]. Table 1 lists the mineralogical and metallurgical characteristics of some of the aforementioned processing plants.

**Table 1.** Main ore and gangue minerals and typical metallurgical results for some processing plants worldwide.

| Plant | Main Minerals | Main Gangue | Feed $Li_2O$ wt%t | Conc. $Li_2O$ wt% | Beneficiation Method | Reference |
|---|---|---|---|---|---|---|
| Greenbushes, Australia | Spodumene, cassiterite, tantalite | Tur | 4.0 | 7.5–7.7 | Flot/MS/ST | [8] |
| Kings Mountain, CA, USA | Spodumene | Alb, qtz, mus | 1.4–1.5 | 6.3 | Flot | [8] |
| Bernic Lake, MB, Canada | Spodumene, amblygonite, tantalite | Alb, qtz | 3.22 | 7.25 | DMS/GS/ Flot/MS | [8] |
| Bikita, Zimbabwe | Petalite, lepidolite, amblygonite, eucryptite | n.d. | 4.2 | 4.5–7.3 | DMS | [8] |
| Bald Hill, Australia | Spodumene, tantalite | Mus | 1.18 | 6.5 | DMS | [8] |
| CBL, Brazil | Spodumene | n.d. | 1.4 | 5.0 | DMS | [11] |
| Mibra, Brazil | Spodumene, cassiterite, tantalite | Alb, qtz, mus | 1.01 | 5.5 | Flot/MS | [12] |

Alb = Albite, qtz = quartz, mus = muscovite, tur = tourmaline, Flot = flotation, M.S. = magnetic separation, GS = gravity separation, DMS = dense media separation; ST = shaking table; n.d.—information not described.

Several spodumene-processing methods were developed and are described in the literature [13,14]. These include dense media separation (DMS), flotation, and magnetic separation. The applications, as well as challenges of these methods, have been previously discussed in the literature [7,8,15,16].

The DMS circuit usually includes two stages at different dense media specific gravities: the first at a lower specific gravity (~2.7), to reject silicate gangue, and the second at higher specific gravity (~2.9), to produce a high-grade spodumene concentrate. DMS is typically carried out on the −850 + 500 µm fraction; however, it is noteworthy that spodumene needs a high degree of liberation for its effective concentration and recovery. Poor spodumene liberation may result in significant lithium losses to the float product and impinge the use of DMS in processing [16]. Separating Fe-bearing minerals from spodumene can be difficult using DMS or flotation

Flotation is used in processing of spodumene pegmatite ores where the average particle size or difference in specific gravities between gangue minerals is too small for efficient gravity separation [8]. The gangue minerals present affect the flotation method. Presence of heavy metal cations have shown to impact the flotation properties of spodumene [7].

Fe-bearing minerals, such as amphibole and tourmaline, are difficult to separate from spodumene by DMS or flotation [8]; hence, magnetic separation can be used prior to flotation to remove large quantities of Fe-bearing minerals. However, it is common to perform after flotation to produce a low iron content concentrate suitable for ceramics and glass manufacturing [16].

Customer specifications of spodumene concentrates vary between technical- and chemical-grade applications. Aspects such as impurities in the spodumene crystal and spodumene particle-size distribution ought to be considered for the intended end use of the concentrate [7,16]. In general, technical-grade spodumene concentrates require low Fe (<0.25%) and $Li_2O$ contents, varying from 5% to 7.5%, and are mainly used in the glass/ceramics industry and metallurgical applications. Chemical-grade spodumene concentrates require an $Li_2O$ content of more than 6.0% with an Fe content of less than

1%–1.5%. They are mainly used in the manufacturing of Li-ion batteries [15,17]. As an example, specifications for a premium spodumene concentrate from Albemarle are: $Li_2O$ content $\geq$ 7.2%, $Fe_2O_3$ content $\leq$ 0.1% and grain size of 100% < 500 µm, max. 18% > 212 µm, and min. 60% > 75% [18].

Chemical-grade applications require the extraction of Li from the spodumene crystal structure. This involves heat conversion (1000–1100 °C) of spodumene from the original alpha form to beta form. The latter is a polymorph vulnerable to chemical attacks, allowing for the extraction of Li through leaching by alkaline or acidic processes [19,20].

For chemical-grade concentrates, the presence of iron-bearing silicate minerals can have a detrimental effect on the subsequent roasting processes because, at high temperature, they tend to soften and cause spodumene particles to agglomerate [16]. For technical-grade applications, the presence of iron oxide (as small as 0.4 wt%) in a glass can result in the coloring of the final product and a reduction of the linear transmission of infrared radiation, thereby limiting the use of the metal in cooktops for infrared cooking [21].

Ore characterization studies on Li-enriched pegmatites were performed to guide mineral processing and revealed the locking, liberation, and deportment characteristics of Li between Li-bearing minerals (e.g., spodumene and micas). These characteristics are important, especially when the minerals exhibit distinct physical properties, because they directly influence the interpretation of the Li data collected from the entire rock analyses [22]. However, Li ore is challenging for characterization because conventional analytical techniques (XRF, SEM-EDS) cannot detect Li. Consequently, few related studies are published in the literature [23].

A few researchers characterize Li ores by combining automated mineralogy with other analytical techniques that can detect Li. These approaches include laser-ablation inductively coupled plasma mass spectrometry (LA–ICPMS) [24], time-of-flight secondary ion mass spectrometry (ToF-SIMS), X-Ray Diffraction (XRD) [22,25–28], and laser-induced breakdown spectroscopy (LIBS) [23]. The use of automated mineralogy in evaluating the efficiency of processes, such as magnetic separation and crushing [24,27,29,30] of Li-bearing minerals, are also notable approaches.

This work, conducted on Li-enriched samples from a pegmatite deposit from southern Minas Gerais State in Brazil, aimed in assessing how much Li of the bulk sample is from spodumene, and therefore, actually recoverable. For that, a comprehensive understanding of Li deportment between Li-bearing minerals was necessary. To address this matter, we combined an SEM-based automated mineralogic approach with LA–ICPMS and other analytical techniques. The use of LA–ICPMS allowed us to assess the Li content in other Li-bearing minerals, in addition to spodumene, that cannot be identified by SEM/EDS/WDS. The results highlight the impact of Li-bearing minerals on the recovery of Li and spotlight the importance of determining Li deportment. The data and findings can help guide processing results on an industrial scale.

## 2. Materials and Methods

Ten samples (labelled as MT01–MT10) were collected from different geological segments along a Li-enriched pegmatite body in southern Minas Gerais (Brazil) (Figure 1). The samples were composed of material from one borehole or combinations of up to three boreholes. A complete flowchart of the applied methodology is presented in Figure 2.

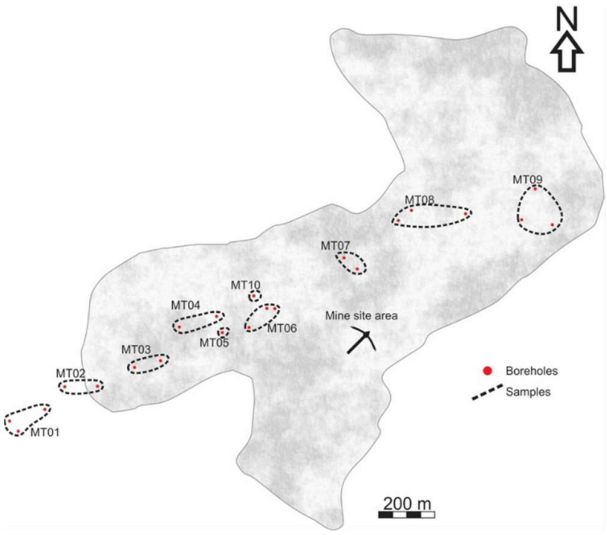


**Figure 1.** Schematic mine site map showing the relative geographic location of the boreholes and samples.

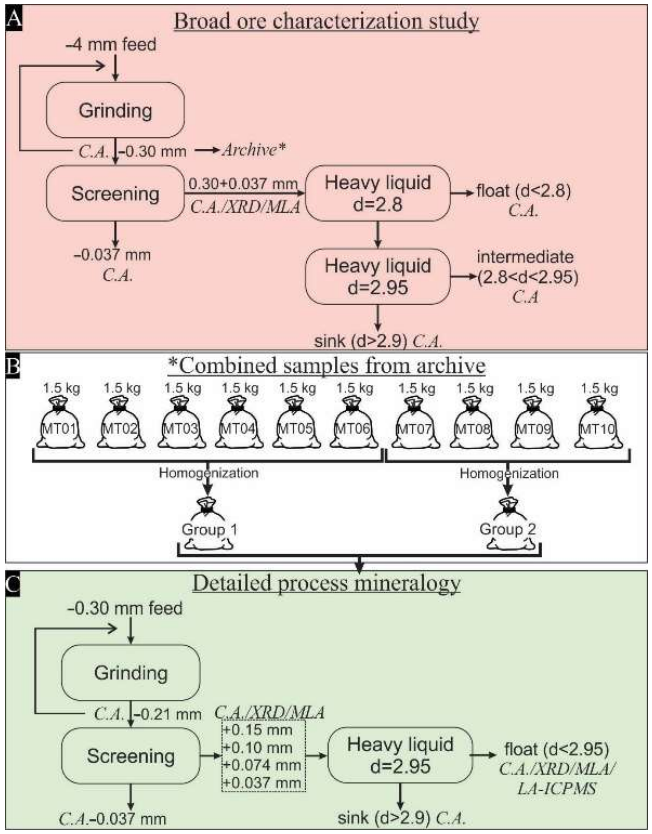


**Figure 2.** Experiment flowchart: (**A**)—Broad ore characterization study performed on 10 samples. (**B**)—Ten samples combined into two groups based on the results of the characterization study. (**C**)—Detailed process mineralogy study performed on two samples. CA—Chemical analysis; XRD—X-ray diffraction; MLA—Mineral liberation analysis; LA–ICPMS—laser ablation inductively coupled plasma mass spectrometry.

### *2.1. Broad Ore Characterization Study*

For the first characterization step, 10 samples containing approximately 30 kg of crushed pegmatite rocks were ground to a size below 4 mm. Representative subsamples of approximately 2.5 kg were collected and then optically assessed to determine spodumene grain size to further grind the subsamples closer to the spodumene's grain size, increasing its liberation from the particles. Spodumene grains of roughly 0.30 mm were observed; therefore, grinding under 0.30 mm was performed in a rod mill, followed by wet screening with a screen aperture of 0.30 and 0.037 mm to remove the fine fraction. Textural analysis in the size of 0.30–0.037 mm was conducted using SEM-based automated mineralogy supported by X-ray diffraction (XRD) to assess the mineral composition and spodumene locking and liberation characteristics. Mineral density separation (fraction 0.30–0.037 mm) was performed using heavy liquids (bromoform $CHBr_3$ at d = 2.8 and tetrabromoethane $C_2H_2Br_4$ at d = 2.95) for obtaining the following products, namely, float (d < 2.8), intermediate (2.8 < d < 2.95), and sink (d > 2.95), the latter representing the spodumene concentrate. Subsamples of the 0.30–0.037 mm and −0.037 mm size fractions and heavy liquid products were transferred to chemical analysis (XRF, ICP-OES).

### *2.2. Detailed Process Mineralogy*

For detailed characterization, 10 samples were combined in two groups (G1 and G2) based on the results of the broad ore characterization study, considering mineralogical and chemical composition, density separation results, and geographic location. The procedure of the process mineralogy studies comprised milling samples below 0.21 mm in a rod mill (based on SEM-based spodumene liberation observation carried out at the broad characterization). Wet screening was performed with screen apertures of 0.21, 0.15, 0.10, 0.074, and 0.037 mm. Chemical analysis of samples under all size fractions were performed. Detailed mineralogical studies using SEM–based image analysis (SEM-IA at MLA system) with XRD support were conducted in all fractions over 0.037 mm. Mineral density separation was performed using tetrabromoethane ($C_2H_2Br_4$ (at = 2.95) to assess the spodumene concentrate in terms of Li content and deportment. Additionally, the effect of other Li-bearing minerals in the test was assessed. Detailed mineralogical studies were performed on the float product (d < 2.95) using SEM-IA. Selected grains of Li-bearing minerals from the float product of the coarser fraction (+0.15 mm) were evaluated by LA–ICPMS to assess their Li content and determine Li deportment by density.

### *2.3. Analytical Techniques*

XRF, ICP–OES, XRD, and SEM-IA were performed at the Multiuser Center of the Technological Characterization Laboratory at University of São Paulo (LCT–USP). Meanwhile, LA–ICPMS analysis was performed at the NAP Geoanalítica-USP (Geoanalytical Research Support Center, Geosciences Institute, University of São Paulo, São Paulo, Brazil).

#### 2.3.1. Chemical Analysis

Quantitative chemical analyses were performed under XRF (Zetium, Panalytical, Malvern, UK) to determine the major elements (i.e., Si, Fe, Al, Ca, Mg, Na, K, F, Rb) using molten inserts compared with a certified reference material (AMIS 0355). Loss on ignition was assessed by gravimetry at 1020 °C for 2 h. The Li content was assessed by ICP–OES (Horiba Ultimate Expertz, Kyoto, Japan) using samples prepared through fusion with borax ($Na_2[B_4O_5(OH)_4]\cdot 8H_2O$).

#### 2.3.2. XRD

Mineralogical analyses were performed by XRD using the powder method in a Bruker D8 Endeavor diffractometer (Co Kα, step 0.02°, 38 s/step, scanning from 2 to 70°2θ). The mineral was identified on the X'Pert Highscore Plus 4.8 (Malvern Panalytical, Malvern, UK) software by comparing the diffractograms with the PDF2 dataset of the International Centre for Diffraction Data (angle 2–70°, step 0.02, time 38 s/step).

#### 2.3.3. SEM-Based Automated Mineralogy (SEM-IA)

Polished section mounts of samples G1 and G2 (except −0.037 mm) were prepared by size fraction to determine the relationship between gangue minerals and spodumene using a SEM Quanta 650FEG Thermo/FEI and an SEM–IA with MLA system [31] coupled with EDS (Esprit Bruker Nano Analytics, Billerica, MA, USA) system. To perform the SEM–IA, we used the GXMAP measurement mode. GXMAP uses X-ray mapping in phases that cannot be segmented solely by backscattering image (BSE) grey levels and employs a faster area X-ray analysis for phases that are readily segmented [31]. To accurately differentiate minerals with similar atomic number (e.g., quartz and plagioclase), the contrast was set high, allowing the MLA to easily identify several grey levels and then separate them by their chemical composition (characteristic X-ray spectra) using EDS. To identify minerals with higher atomic numbers (e.g., cassiterite, tantalite, and microlite), an X-ray mapping trigger was set for minerals with a grey level of over 250.

The chemical composition and characteristic X-ray of each mineral was input to the MLA database; for that, several mineral grains were chemically analyzed using the LEO Stereoscan 440 SEM with an EDS detector (INCA X-act, Oxford) calibrated with certified reference standards.

The MLA calculated the modal mineral content (in mass) of a phase based on an area percentage in the polished section mounts using the density of each mineral. The reliability of the data calculated by the MLA was compared with that obtained by the chemical analysis, and an $R^2$ value was assigned to the major elements of each sample. Some fluctuations in the $R^2$ value were due to mineral composition variations that were not modeled, such as Li, Fe, Na, K, $SiO_2$, and Al contents in mica.

#### 2.3.4. LA–ICPMS

Owing to its low energy characteristic X-rays, Li cannot be detected by standard energy-dispersive X-ray spectrometers mounted on electron microscopes. Therefore, in micas, Li was quantified by LA–ICPMS with a Laser New Wave UP-213A/F 213 nm coupled with a Perkin Elan-6100DRC quadrupole ICPMS (spot diameter of 30 µm, frequency of 15 Hz, fluence of 1.13 j/cm$^2$, ablation of 30 s, and baseline of 15 s) operating in a He + Ar atmosphere. The grain composition was determined using the NIST610 standard and Si-standardized stoichiometry for each mineral derived from the data of the EDS analyses.

## 3. Results and Discussion

### *3.1. Broad Ore-Characterization Study*

Table 2 lists the bulk chemical compositions of all samples (MT01–MT10). The average $Li_2O$ content is 1.05 wt%. The $Fe_2O_3$ content ranges from 0.20 to 1.10 wt%, and the CaO content ranges from 0.30 to 1.30 wt%. The $Rb_2O$ content ranges from 0.38 to 1.14 wt%. All samples have similar $SiO_2$, $Al_2O_3$, $Na_2O$, $K_2O$, and MnO contents, averaging approximately 73.0, 15.5, 4.35, 2.00, and 0.15 wt%, respectively.

**Table 2.** Bulk chemical analysis of the samples and SEM-based mineralogical composition of the samples in the fraction of 0.30–0.037 mm.

| | | MT01 | MT02 | MT03 | MT04 | MT05 | MT06 | MT07 | MT08 | MT09 | MT10 |
|---|---|---|---|---|---|---|---|---|---|---|---|
| Compounds (%w; XRF / ICP OES) | $LiO_2$ | 1.08 | 1.45 | 1.74 | 1.43 | 0.25 | 1.51 | 0.93 | 0.75 | 0.75 | 0.58 |
| | $SiO_2$ | 70.50 | 74.50 | 71.10 | 73.50 | 71.90 | 73.40 | 74.30 | 71.70 | 73.70 | 73.60 |
| | $Fe_2O_3$ | 0.28 | 0.20 | 0.43 | 0.28 | 0.51 | 0.45 | 0.65 | 0.65 | 0.81 | 1.10 |
| | $Al_2O_3$ | 16.86 | 15.09 | 6.98 | 15.48 | 16.22 | 15.49 | 15.02 | 16.16 | 15.59 | 13.37 |
| | CaO | 0.36 | 0.30 | 0.63 | 0.32 | 0.31 | 0.34 | 0.64 | 0.46 | 0.63 | 1.30 |
| | MgO | <0.01 | <0.01 | <0.01 | <0.01 | <0.01 | <0.01 | <0.01 | <0.01 | 0.36 | 0.34 |
| | $Na_2O$ | 4.52 | 3.94 | 3.55 | 4.11 | 4.42 | 3.62 | 4.72 | 5.11 | 4.91 | 4.68 |
| | $K_2O$ | 2.66 | 1.63 | 1.78 | 1.68 | 1.23 | 1.85 | 1.64 | 1.90 | 1.71 | 1.14 |
| | F | 1.03 | 0.71 | 0.92 | 0.44 | - | - | - | - | - | - |
| | $Rb_2O$ | 1.14 | 0.84 | 0.91 | 0.66 | 0.32 | 0.66 | 0.49 | 0.45 | 0.50 | 0.38 |

**Table 2.** *Cont.*

| | | MT01 | MT02 | MT03 | MT04 | MT05 | MT06 | MT07 | MT08 | MT09 | MT10 |
|---|---|---|---|---|---|---|---|---|---|---|---|
| Minerals (%) | quartz | 30.02 | 37.66 | 31.08 | 34.57 | 40.10 | 33.55 | 33.84 | 31.85 | 32.55 | 39.64 |
| | albite | 33.81 | 29.22 | 26.94 | 29.46 | 39.68 | 28.10 | 38.36 | 40.16 | 39.77 | 37.79 |
| | mica | 27.28 | 19.02 | 19.84 | 16.38 | 14.03 | 16.05 | 13.10 | 16.11 | 14.26 | 10.73 |
| | spodumene | 6.83 | 12.94 | 18.77 | 17.90 | 2.88 | 19.30 | 10.38 | 6.89 | 9.14 | 5.02 |
| | K-feldspar | 0.83 | 0.42 | 0.38 | 0.88 | 0.20 | 1.83 | 1.77 | 2.79 | 1.93 | 0.88 |
| | epidote | 0.27 | 0.16 | 2.14 | 0.30 | 0.32 | 0.66 | 1.83 | 1.19 | 0.89 | 4.71 |
| | garnet | 0.09 | 0.03 | 0.05 | 0.11 | 0.10 | 0.06 | 0.18 | 0.24 | 1.03 | 0.66 |
| | apatite | 0.24 | 0.14 | 0.25 | 0.16 | 0.12 | 0.20 | 0.26 | 0.14 | 0.19 | 0.34 |
| | cassiterite | 0.23 | 0.02 | 0.02 | 0.01 | 0.01 | 0.03 | 0.06 | 0.04 | 0.07 | 0.05 |
| | kaolinite | 0.01 | 0.02 | 0.05 | 0.02 | 2.24 | 0.01 | 0.01 | 0.44 | 0.01 | 0.00 |
| | microlite | 0.06 | 0.18 | 0.20 | 0.08 | 0.03 | 0.03 | 0.07 | 0.05 | 0.06 | 0.05 |
| | coltan | 0.01 | 0.00 | 0.13 | 0.01 | 0.06 | 0.01 | 0.02 | 0.02 | 0.04 | 0.02 |
| | Other * | 0.30 | 0.18 | 0.13 | 0.10 | 0.22 | 0.17 | 0.09 | 0.07 | 0.05 | 0.10 |

* Other: sphalerite, gibbsite, fluorite, barite.

Table 2 lists the SEM-IA results based the mineralogical compositions of samples in the fraction of 0.30–0.037 mm. In general, the samples are made up of quartz (average 34.5%), plagioclase (average 34.3%), and mica (average 16.7%). Spodumene content ranges from 2.88% in sample MT05 to 19.3% in sample MT06. Sample MT01 has 27.3% mica content while all other samples average 15.5% mica content.

Table 3 lists the chemical results based on the SEM-IA area percentage of minerals and an assumed density for each mineral compared with the results of the chemical analysis of the major elements in the same size fraction. The correlation coefficient ($R^2$) between the SEM-IA calculated and chemically measured compound content indicates the deviation of the results from a perfectly linear relationship. As indicated in the table, the analysis presents an $R^2$ value of 0.99, which indicates a good correlation between the calculated and measured data. The differences in $Li_2O$, $Fe_2O_3$, CaO, and $K_2O$ are due to the varying mineral compositions that could not be measured, as the mineral classification data input requires a fixed mineral composition.

**Table 3.** Calculated SEM-IA vs. measured chemical analysis data for the 0.30–0.037 mm fraction.

| Element | | Compound (%w; XRF/ICP–OES) | | | | | | |
|---|---|---|---|---|---|---|---|---|
| | | $Li_2O$ | $Fe_2O_3$ | $SiO_2$ | $Al_2O_3$ | CaO | $K_2O$ | $R^2$ |
| MT01 | SEM-IA | 1.14 | 0.07 | 70.86 | 18.19 | 0.41 | 3.00 | 0.99 |
| | CA | 1.01 | 0.26 | 70.08 | 16.95 | 0.24 | 2.77 | |
| MT02 | SEM-IA | 1.48 | 0.06 | 75.03 | 16.14 | 0.23 | 2.10 | 0.99 |
| | CA | 1.50 | 0.16 | 74.73 | 15.05 | 0.18 | 1.68 | |
| MT03 | SEM-IA | 1.94 | 0.29 | 71.77 | 17.99 | 0.79 | 2.14 | 0.99 |
| | CA | 1.97 | 0.32 | 71.32 | 16.65 | 0.54 | 1.79 | |
| MT04 | SEM-IA | 1.78 | 0.10 | 74.53 | 16.61 | 0.21 | 1.85 | 0.99 |
| | CA | 1.64 | 0.39 | 75.64 | 14.81 | 0.26 | 1.85 | |
| MT05 | SEM-IA | 0.40 | 0.18 | 77.00 | 13.89 | 0.24 | 1.30 | 1.00 |
| | CA | 0.28 | 0.47 | 77.36 | 13.70 | 0.26 | 1.35 | |
| MT06 | SEM-IA | 1.90 | 0.22 | 73.96 | 16.88 | 0.35 | 1.98 | 0.99 |
| | CA | 1.68 | 0.38 | 76.86 | 14.73 | 0.31 | 1.92 | |
| MT07 | SEM-IA | 1.07 | 0.32 | 74.52 | 15.59 | 0.68 | 1.59 | 0.99 |
| | CA | 0.84 | 0.53 | 76.88 | 13.78 | 0.56 | 1.63 | |
| MT08 | SEM-IA | 0.85 | 0.29 | 73.57 | 16.17 | 0.43 | 2.07 | 0.99 |
| | CA | 0.68 | 0.59 | 75.73 | 14.62 | 0.37 | 2.05 | |
| MT09 | SEM-IA | 0.97 | 0.25 | 74.09 | 15.80 | 0.48 | 1.72 | 0.99 |
| | CA | 0.77 | 0.55 | 76.49 | 14.49 | 0.52 | 1.62 | |
| MT10 | SEM-IA | 0.58 | 0.56 | 76.03 | 3.95 | 1.54 | 1.18 | 0.99 |
| | CA | 0.53 | 0.83 | 77.54 | 12.62 | 1.14 | 1.19 | |

CA—chemical analysis.

The mineral compositions of samples MT01–M06 resemble the Greenbushes deposit (Bale and May, 1989 [9]), Pilangoora Project [26], and Bald Hill deposits in Australia [8], with spodumene as the main Li ore mineral, in addition to cassiterite and tantalite. In terms of chemical composition, samples MT01–MT06 have $Li_2O$ content common to other Li deposits worldwide, including Kings Mountain (1.4–1.5 wt% $Li_2O$) [32] and Bald Hill (1.18 wt% $Li_2O$) (Tadesse et al., 2019 [8]). Further, samples MT07–MT10 have a smaller $Li_2O$ content than typical Li pegmatite deposits (< 1.0 wt% $Li_2O$).

In the density separation process, the sink product of samples MT01–MT06 exhibited lower $Li_2O$ deportment (approximately 40%) with a grade of approximately 6.9 wt%. These samples (except MT05) were observed to have a bulk $Li_2O$ > 1 wt%, $Fe_2O_3$ < 0.5 wt%, and mica > 14% in the fraction of –0.30 + 0.037 mm. Samples MT07–MT10 showed higher $Li_2O$ deportment in the sink product (approximately 60%) with a grade of approximately 5.4 wt% (Figure 3). These samples (and sample MT05) were observed to have a bulk $Li_2O$ < 1.00 wt%, $Fe_2O_3$ > 0.60 wt%, and mica < 16.0% in the size fraction of –0.30 + 0.037 mm.

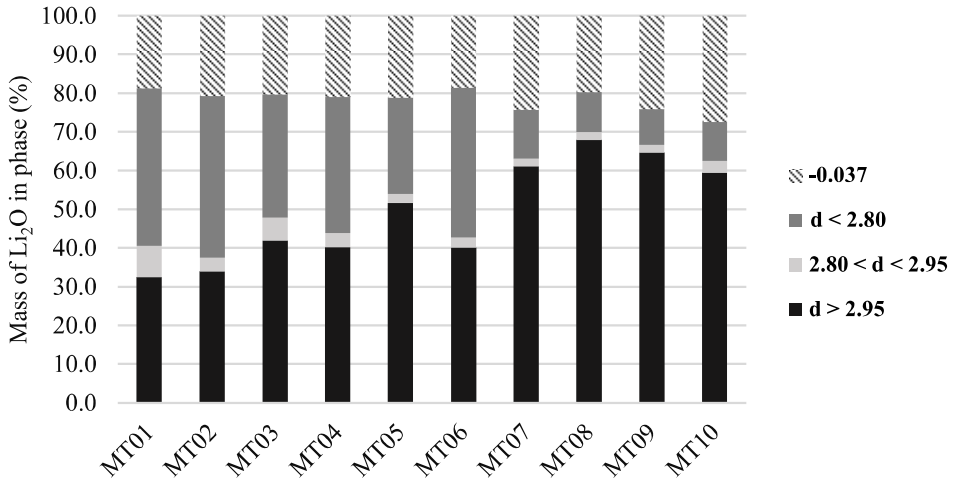


**Figure 3.** Mass percentage of $Li_2O$ in the density separation products and in a fraction under 0.037 mm.

To gain a better understanding of the cause of the lower Li deportment in samples MT01–MT06 and higher deportment in MT07–MT10, the quantitative locking and liberation characteristics of spodumene and content of Li in other minerals were assessed.

### *3.2. Combined Samples*

The trends observed in the bulk chemical composition show that samples MT01-MT04 and MT06 have similarities which can be observed in the correlation graphs between $Li_2O$ and $SiO_2$, $Al_2O_3$, $Fe_2O_3$, and $Rb_2O$ (Figure 4a–d). Samples MT03, MT04, and MT06 have higher spodumene content (approximately 19%), reaching up to twice as much as the other samples. Sample MT01 has almost twice as much mica (27%) as the other samples.

Considering these observations and the Li distribution by density separation products results, samples MT01–MT06 were combined to form G1 and MT07–MT10 to form G2. Although MT05 had lower $Li_2O$ and spodumene contents (0.25 wt%, Figure 4a, and 2.9%, respectively) than those in samples MT01–MT04 and MT06 ($Li_2O$ > 1.00 wt%, $Fe_2O_3$ < 0.50%, Figure 4c), it was considered a part of G1 because of its geographic location along the pegmatite vein. MT05 is closer to the samples in this group and, from a mining perspective, this block would end up together with the samples in G1.

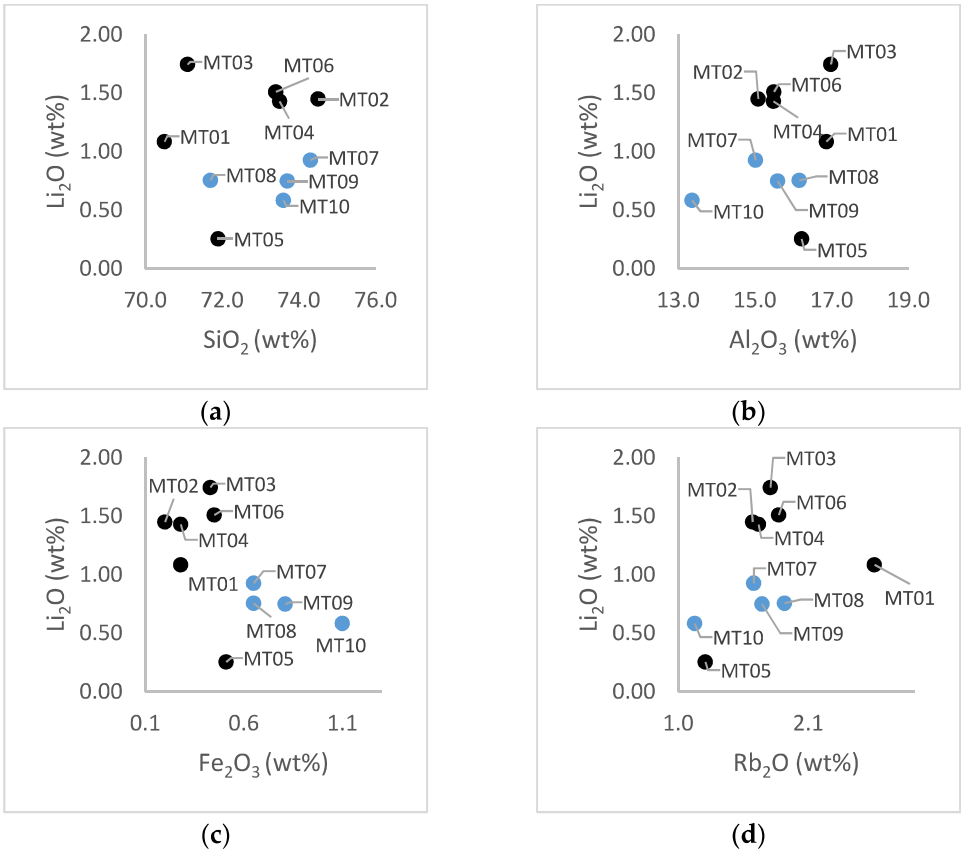


**Figure 4.** Chemical correlation between $Li_2O$ and $SiO_2$ (**a**), $Al_2O_3$ (**b**), $Fe_2O_3$ (**c**), and RbO (**d**). Black dots represent samples in G1 and blue dots samples in G2.

### *3.3. Detailed Process Mineralogy*

This section details the ore characterization study performed across five size fractions for samples G1 and G2.

#### 3.3.1. Sample Composition and Distribution by Size Fractions

Table 4 lists the chemical composition of the major compounds of G1 and G2. On the one hand, G1 has a high bulk $Li_2O$ content (1.26 wt%) but low $Fe_2O_3$ (0.32 wt%) and CaO (0.62 wt%) contents. On the other hand, G2 has a lower bulk $Li_2O$ content (0.62 wt%) and the $Fe_2O_3$ (0.74 wt%) and CaO (0.76 wt%) contents are almost twice as high as in G1.

**Table 4.** Bulk chemical analysis of G1 and G2.

| | Compound (wt%; XRF/ICP–OES) | | | | | | | | | |
|---|---|---|---|---|---|---|---|---|---|---|
| **Element** | **$LiO_2$** | **$Fe_2O_3$** | **$SiO_2$** | **$Al_2O_3$** | **CaO** | **MgO** | **MnO** | **$Na_2O$** | **$K_2O$** | **LOI** |
| Group 1 | 1.26 | 0.32 | 73.0 | 15.6 | 0.43 | <0.10 | 0.17 | 3.74 | 1.76 | 2.73 |
| Group 2 | 0.62 | 0.74 | 74.0 | 14.5 | 0.76 | 0.20 | 0.11 | 4.56 | 1.55 | 2.36 |

The sieve analysis showed that approximately 27% of the samples' masses report to the finer fraction (–0.037 mm) in both groups. The $Li_2O$ content in this fraction in G1 is 1.09 wt% and 0.63 wt% in G2, accounting for 23% and 25% of Li deportment, respectively (Table 5).

**Table 5.** Mass retained (%), compound content (wt%), and deportment (%) by size fraction.

| Fraction (mm) | Mass Retained (%) | | Compound (wt%) | | | | | | Deportment (%) | | | | | |
|---|---|---|---|---|---|---|---|---|---|---|---|---|---|---|
| | | | $Li_2O$ | | $Fe_2O_3$ | | CaO | | $Li_2O$ | | $Fe_2O_3$ | | CaO | |
| | G1 | G2 | G1 | G2 | G1 | G2 | G1 | G2 | G1 | G2 | G1 | G2 | G1 | G2 |
| −0.21 + 0.15 | 24.3 | 22.7 | 1.45 | 0.75 | 0.28 | 0.58 | 0.26 | 0.52 | 27.5 | 25.2 | 20.1 | 17.5 | 14.8 | 15.3 |
| −0.15 + 0.105 | 17.3 | 16.3 | 1.38 | 0.66 | 0.26 | 0.50 | 0.30 | 0.57 | 18.6 | 16.0 | 13.3 | 10.8 | 12.2 | 12.1 |
| −0.105 + 0.074 | 11.4 | 12.2 | 1.26 | 0.65 | 0.26 | 0.56 | 0.33 | 0.67 | 11.2 | 11.7 | 8.74 | 9.07 | 8.81 | 10.6 |
| −0.074 + 0.037 | 20.6 | 22.1 | 1.25 | 0.68 | 0.32 | 0.70 | 0.44 | 0.81 | 20.0 | 22.1 | 19.5 | 20.6 | 21.2 | 23.2 |
| −0.037 | 26.5 | 26.7 | 1.09 | 0.63 | 0.49 | 1.18 | 0.69 | 1.12 | 22.6 | 25.0 | 38.4 | 42.0 | 42.9 | 38.8 |
| Total + 0.037 | 73.5 | 73.3 | 1.34 | 0.69 | 0.28 | 0.60 | 0.33 | 0.64 | 77.4 | 75.0 | 61.6 | 58.0 | 57.1 | 61.2 |
| Total sample | 100 | 100 | 1.28 | 0.68 | 0.34 | 0.75 | 0.43 | 0.77 | 100 | 100 | 100 | 100 | 100 | 100 |

In the fraction of 0.30–0.037 mm, the $Li_2O$ contents in G1 and G2 are 1.35 wt% and 0.69 wt%, accounting for 77% and 75% of lithium's deportment, respectively. The $Fe_2O_3$ (0.60 wt%) and CaO (0.64 wt%) contents in this interval are two times higher in G2 than that in G1 (Table 5). Figure 5 illustrates the Li distribution by the sieve size and the Li content in the total +0.037 mm fraction for both groups.

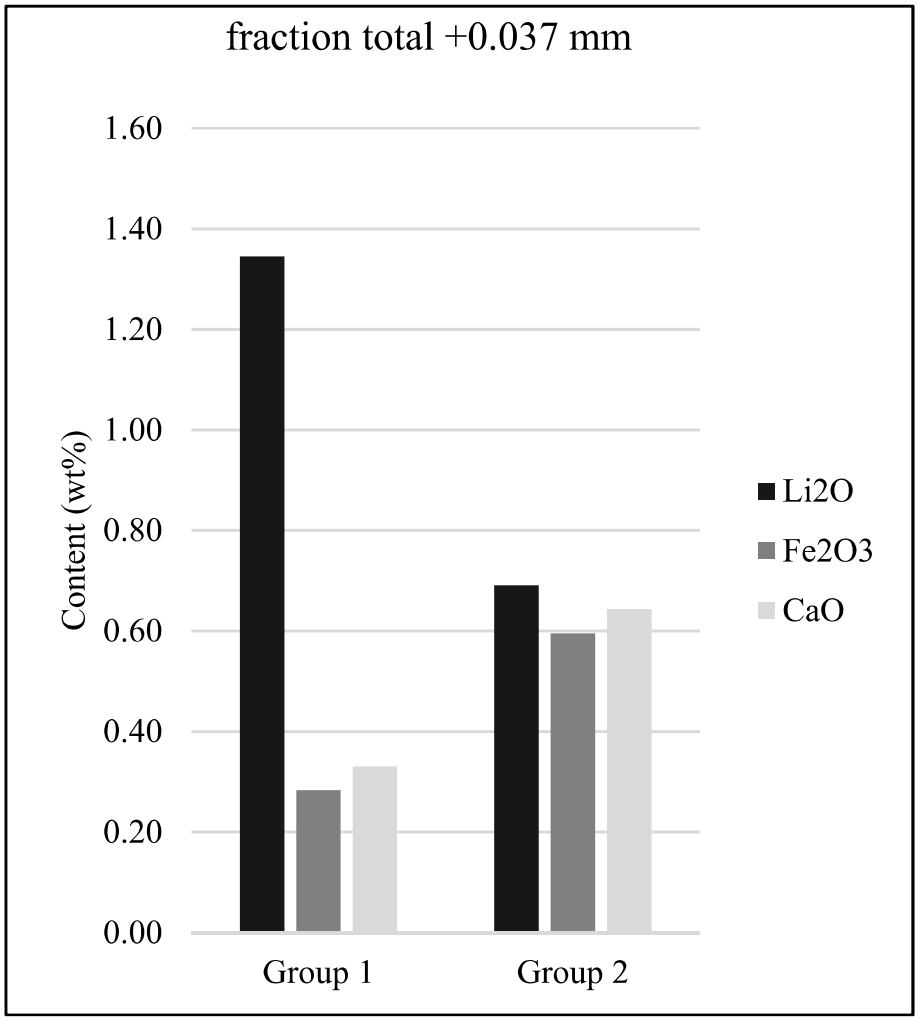


**Figure 5.** $Li_2O$, $Fe_2O_3$, and CaO contents in the size fraction of total +0.037 mm.

### 3.3.2. Mineralogical Composition

Figure 6 illustrates the mineralogical composition of G1 and G2. Both groups present a similar composition with mainly quartz, plagioclase, spodumene, muscovite, lepidolite, and K-feldspar. G1 has 5% more spodumene, 3% more muscovite, and 5% more lepidolite than G2, whereas G2 has slightly more epidote and other minerals than G1, which include Fe-bearing minerals such as garnet and amphibole. This can be detrimental in the subsequent processing steps as separating Fe-bearing minerals from spodumene can be difficult using DMS or flotation.

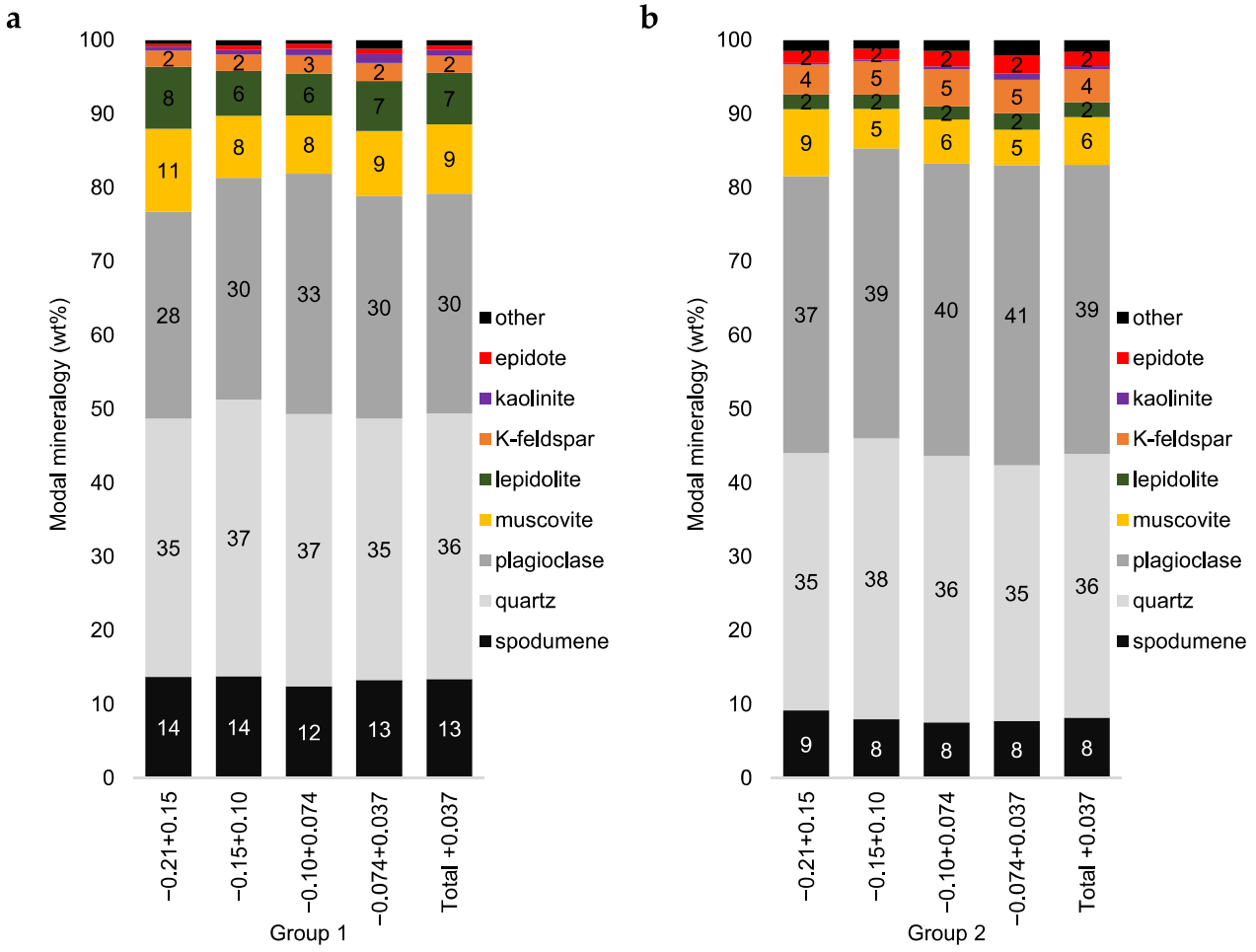


**Figure 6.** Modal mineralogy obtained by SEM-IA for G1 (**a**) and G2 (**b**).

### 3.3.3. Morphology and Microstructure of Spodumene

Figure 7 depicts the representative mineral composition maps of the coarser sized fraction (−0.21 + 0.15 mm) and an enlarged view of the spodumene grain relationships with other minerals. G1 and G2 are abundant in liberated spodumene grains, often appearing in a tabular form. Quartz, plagioclase, muscovite, and lepidolite are generally present as gangue minerals. Moreover, K-feldspar is observed in G2 (Figure 7a,c,e,f). The magnified images reveal associations of spodumene grains with plagioclase and muscovite in G1 (Figure 7b,d) and with plagioclase, quartz, and lepidolite in G2 (Figure 7d,h). Muscovite appears to occur mainly along the margins and fractures of the spodumene grains.

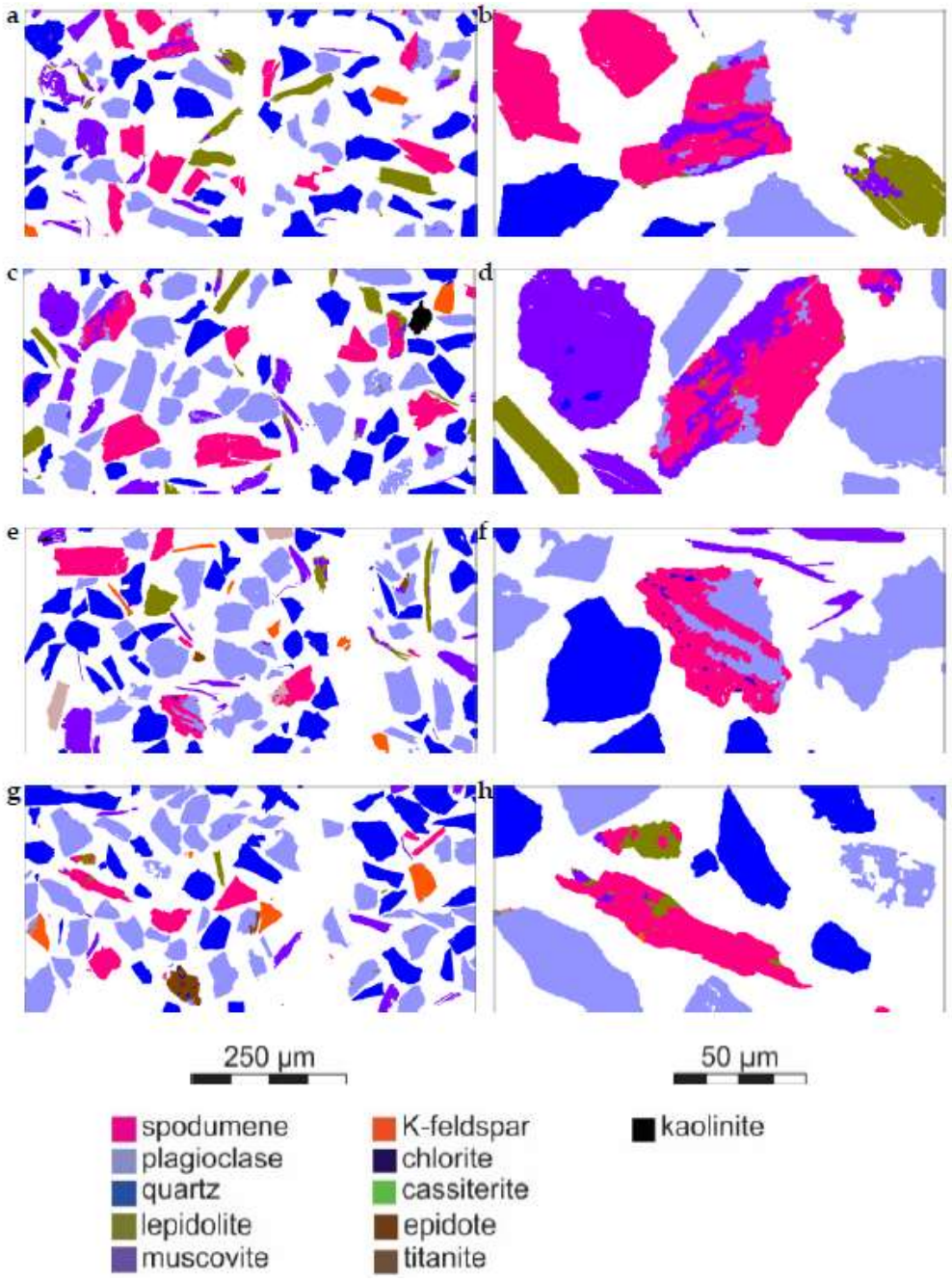


**Figure 7.** MLA mineral composition maps highlighting liberated spodumene and gangue mineral grains in the −0.21 + 0.15 mm size fraction for G1 (**a**,**c**) and G2 (**e**,**g**). The mineral maps on the right size show an enlarged view of the different mineral textures in some spodumene grains from G1 (**b**,**d**) and G2 (**f**,**h**).

The mineralogical transformation of spodumene into micaceous minerals reduces its density, and it therefore reduces the density differences between spodumene and gangue minerals, affecting DMS results. Additionally, spodumene tends to break into acicular particles that easily float with gangue minerals [33].

3.3.4. Mineral Liberation and Locking Characteristics

Figure 8 depicts the liberation characteristics of spodumene in both groups. The level of locking is expressed as a function of the area of spodumene. Liberated spodumene particles contain ≥ 95% of spodumene by area. Binary particles are composed of spodumene associated with one other mineral phase, and complex particles are composed of spodumene and two or more different mineral phases.

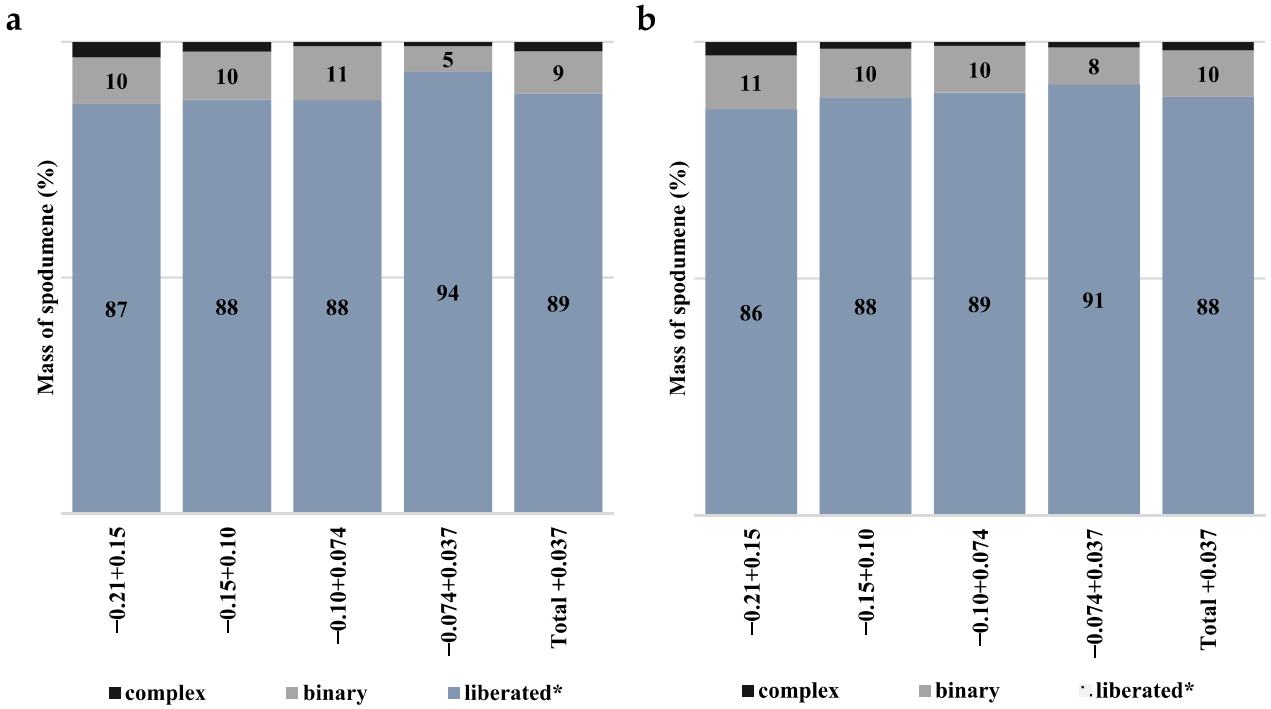


**Figure 8.** Spodumene liberation characteristics for G1 (**a**) and G2 (**b**). Liberation is based on spodumene area (liberated ≥ 95% spodumene). Binary particles are composed of spodumene and another mineral phase, whereas complex particles are composed of spodumene and two or more different mineral phases. *: Grains with ≥95% spodumene in area.

The global liberation of spodumene (total +0.037 mm) in G1 and G2 are 89% and 88%, respectively, ranging from approximately 86% in the coarser size fraction to 94% in the finer size fractions. In both groups, binary particles are more common (approximately 9%) than complex ones (approximately 2%). The most relevant associations of spodumene, either binary or complex, are with mica (muscovite + lepidolite), plagioclase, and quartz.

Results showed that spodumene was fairly liberated by area, which implies that further processing with DMS should efficiently separate most gangue minerals (quartz, plagioclase, and mica) from spodumene.

Figure 9a,b illustrate the liberation characteristics of spodumene for both groups in terms of liberated free surface area. Liberation by free surface is important for further processing because it provides information on the surface area available for a leaching solution to reach or a collector/depressant to attach. In general, G2 exhibits slightly higher surface exposure than G1. In the size fraction of total + 0.037 mm, spodumene particles with ≥ 95% of free surface area represent approximately 83% in G1 and 87% in G2. Moreover, higher surface exposure is observed in these particles toward finer size fractions. Only in this size fraction does G1 have slightly higher surface exposure than G2.

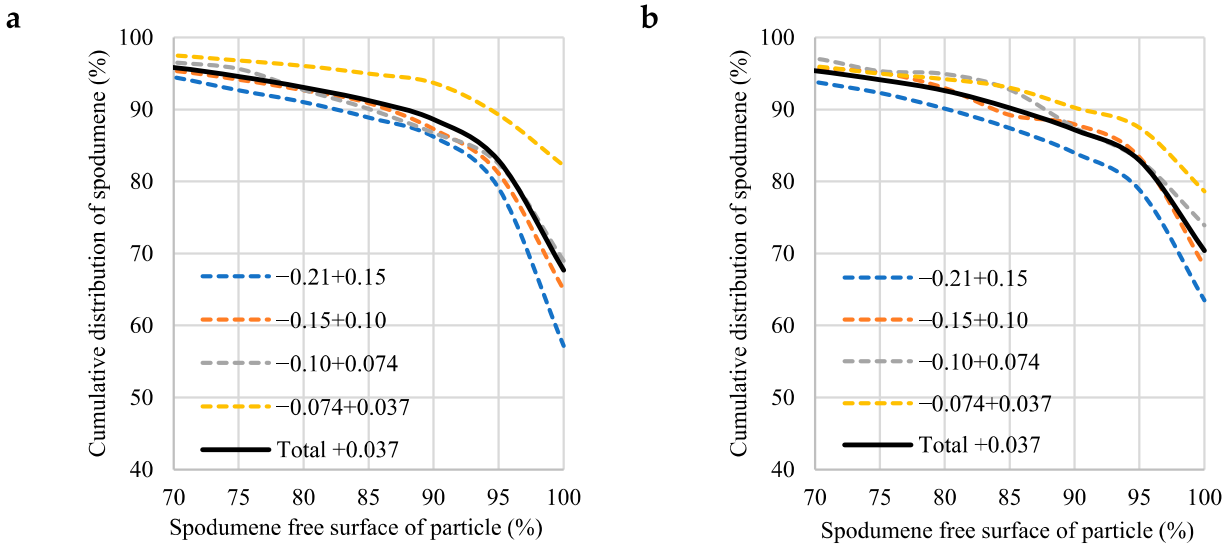


**Figure 9.** Mineral liberation by free surface area for spodumene in G1 (**a**) and G2 (**b**).

### 3.3.5. Theoretical Grade Recovery Curve

The theoretical grade–recovery curve is defined as the maximum expected recovery that can be achieved by physical separation of a mineral at a given grade [34], and it is determined by the surface area liberation of the mineral of interest, which is directly related to the grind size [26]. As the liberation results were obtained by 2D measurements, the true liberation results were overestimated; therefore, they can only serve as a guide [35].

Figure 10 illustrates the theoretical grade–recovery curves for spodumene in G1 and G2. At a spodumene recovery rate of 70%, a pure spodumene concentrate with an $Li_2O$ content of 8.01 wt% is achievable in both samples. At a spodumene recovery rate of 90%, a grade of approximately 7.4 wt % $Li_2O$ is expected in a coarser size fraction, while it increases up to 7.8 wt% $Li_2O$ in a finer one.

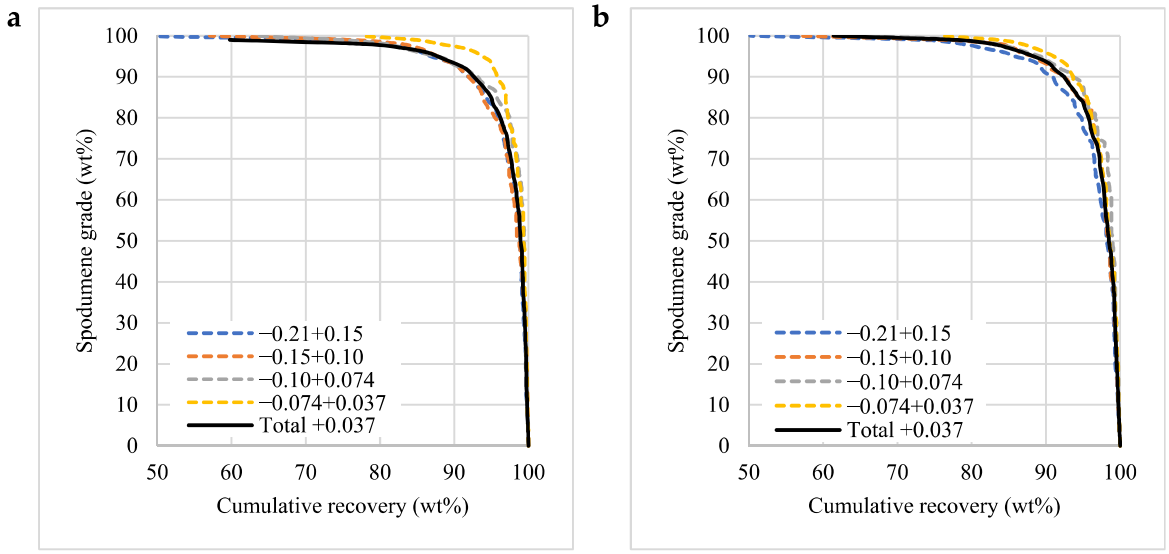


**Figure 10.** Theoretical grade recovery curves for spodumene in G1 (**a**) and G2 (**b**).

3.3.6. Mica Composition

In both groups, two types of micas were distinguished by SEM-IA and classified as muscovite and lepidolite. No differences in the micaceous compositions were observed between the samples; variations were found only in the abundance of micas.

Figure 11a illustrates the SEM-IA mineral composition map of a mica particle comprising muscovite and lepidolite and presents the difference in the EDS spectra between the two minerals. Figure 10b depicts the same mica particle in a BSE image, in which muscovite has a lower grey level than lepidolite. The EDS analysis was performed next to the black spots, which are laser marks from the LA–ICPMS analysis. The EDS table below the image shows that muscovite (points 13 and 14) has, in general, less $SiO_2$ and more $Al_2O_3$. Lepidolite also contains more $Rb_2O$ and F content.

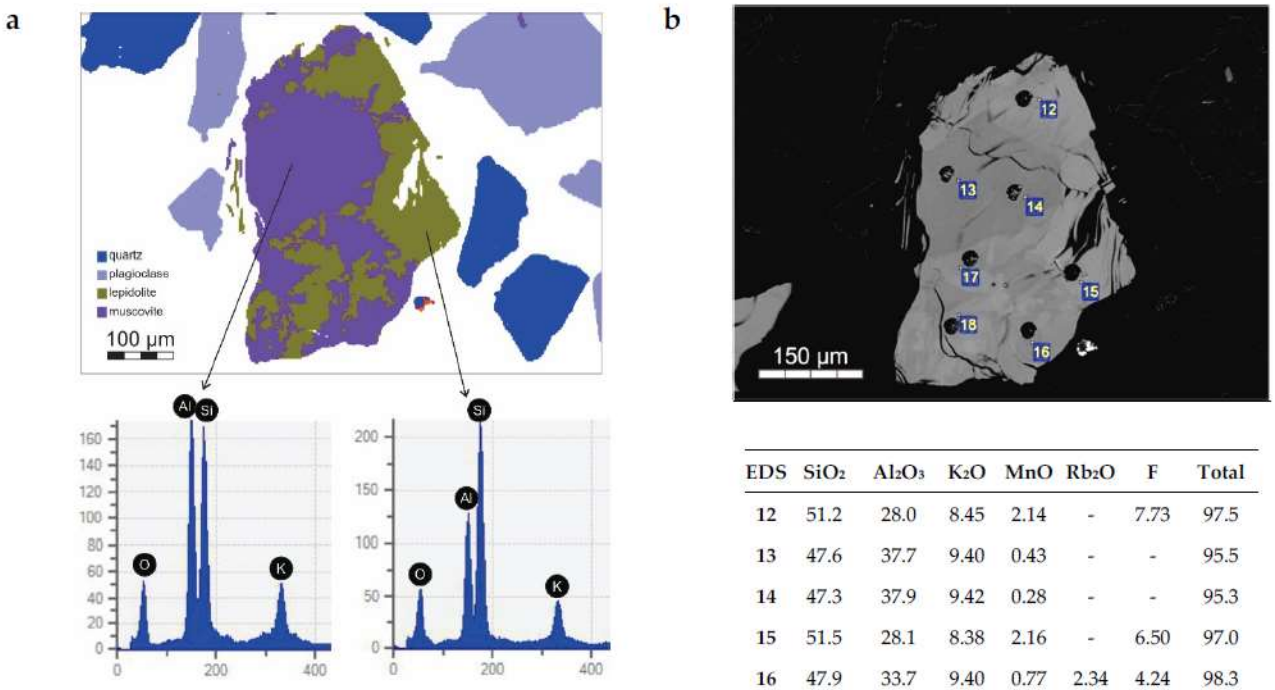


| EDS | $SiO_2$ | $Al_2O_3$ | $K_2O$ | MnO | $Rb_2O$ | F | Total |
|---|---|---|---|---|---|---|---|
| 12 | 51.2 | 28.0 | 8.45 | 2.14 | - | 7.73 | 97.5 |
| 13 | 47.6 | 37.7 | 9.40 | 0.43 | - | - | 95.5 |
| 14 | 47.3 | 37.9 | 9.42 | 0.28 | - | - | 95.3 |
| 15 | 51.5 | 28.1 | 8.38 | 2.16 | - | 6.50 | 97.0 |
| 16 | 47.9 | 33.7 | 9.40 | 0.77 | 2.34 | 4.24 | 98.3 |
| 17 | 47.6 | 31.8 | 9.35 | 1.16 | 2.72 | 5.36 | 98.4 |
| 18 | 49.2 | 30.0 | 9.03 | 1.39 | 3.05 | 5.13 | 98.1 |

**Figure 11.** SEM-IA particle composition map illustrating the X-ray spectrum of each classified phase (**a**) and the BSE image of the same particle depicting the EDS analysis results for each mineral phase (**b**).

Table 6 lists the LA–ICPMS analysis performed on muscovite and lepidolite grains from the floated product of the heavy media test on G1 and G2. A total of 23 measurement points were collected on muscovite and 41 on lepidolite. Muscovite has an $Li_2O$ content of approximately 0.5 wt% and lepidolite has approximately 3.1 wt%. The latter represents a solid solution series between the trilithionite–polylithionite series and siderophyllite [36]; therefore, the $Li_2O$ content fluctuates by a large margin between 1.25 and 5.75 wt% $Li_2O$ in the grains analyzed. As observed in the EDS results, muscovite has a smaller $SiO_2$ content (47.0 wt%) and a larger $Al_2O_3$ content (36.9 wt%) than lepidolite (50.0 wt% $SiO_2$ and 30.9 wt% $Al_2O_3$). Lepidolite has a slightly higher F content (1.56 wt%) than muscovite (0.22 wt%). Both micas have a reasonable content of $Rb_2O$, 3.25 wt% in muscovite and 4.86% in lepidolite.

**Table 6.** Average composition of muscovite and lepidolite grains obtained by LA–ICPMS.

| | Content (wt%) | | | | | | | |
|---|---|---|---|---|---|---|---|---|
| **Muscovite** | **$Li_2O$** | **F** | **$Al_2O_3$** | **$SiO_2$** | **$K_2O$** | **FeO** | **$Fe_2O_3$** | **$Rb_2O$** |
| Mean | 0.48 | 0.22 | 36.9 | 47.0 | 10.1 | 2.33 | 2.61 | 3.25 |
| SD | 0.20 | 0.69 | 1.88 | 1.27 | 0.46 | 1.21 | 1.32 | 0.70 |
| Maximum | 0.95 | 2.78 | 40.8 | 50.28 | 11.2 | 5.47 | 6.08 | 4.23 |
| Minimum | 0.13 | 0.00 | 31.25 | 44.3 | 8.75 | 0.11 | 0.30 | 1.05 |
| Lepidolite | | | | | | | | |
| Mean | 3.10 | 1.56 | 30.9 | 50.0 | 9.83 | 1.26 | 1.28 | 4.86 |
| SD | 1.34 | 2.83 | 3.47 | 2.81 | 0.60 | 1.89 | 2.15 | 0.95 |
| Maximum | 5.75 | 9.49 | 37.3 | 54.10 | 11.2 | 8.76 | 9.73 | 6.67 |
| Minimum | 1.25 | 0.00 | 24.0 | 44.8 | 8.93 | 0.24 | 0.00 | 2.65 |

### 3.3.7. Li Deportment in Li-Bearing Minerals

Li deportment was calculated by considering the LA–ICPMS data and relating it to the modal mineralogy obtained by the MLA for each group. The Li content in spodumene was considered theoretical (8.01 wt% $Li_2O$). In the fraction of total +0.037 mm, the Li content in spodumene, lepidolite, and muscovite accounted for 80, 16, and 3% in G1, and 88, 8, and 4% in G2, respectively (Figure 12).

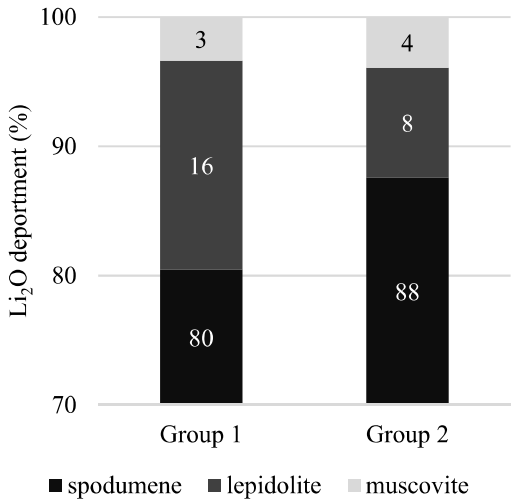


**Figure 12.** Li deportment in the total +0.037 mm interval.

In the total +0.037 mm interval, G1 had a $Li_2O$ content of 1.26 wt%; however, based on the Li deportment values, spodumene contains approximately 1.01 wt% and is therefore considered usable. G2 has an $Li_2O$ content of 0.62 wt% and spodumene contains 0.58 wt%.

### 3.3.8. Density Separation

The density of spodumene is 3.1, whereas most gangue minerals have densities from 2.6 to 3.0. The test was performed at a density of 2.95; therefore, spodumene concentrates in the sunken product, and few other minerals, mainly Fe-bearing ones, should also report to this product. Figure 13 illustrates heavy liquid Li deportment for the fraction of 0.30 + 0.037. On the one hand, the sunken product, G1, has Li deportment of 44% and an $Li_2O$ content of 6.53 wt%. On the other hand, G2 has a lower $Li_2O$ content of 4.92 wt%, but with a higher Li deportment of 58%.

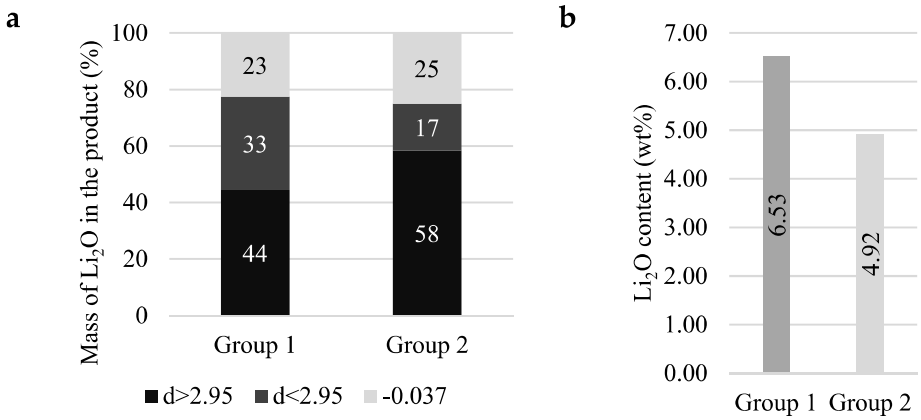


**Figure 13.** Heavy liquid Li deportment in the size fraction of total + 0.037 mm (**a**) and Li content in the sunken product of both samples (**b**).

Both samples present similar high liberation degrees of spodumene (approximately 88%), therefore, the deportment result is not influenced by the liberation degree. In fact, a higher modal presence of Li-bearing micas (9% muscovite and 7% lepidolite) in G1 heavily influenced the Li deportment results, while the lower modal presence of Fe-bearing minerals (<1%) led to the formation of a higher Li content in the sunken product. By contrast, the lower modal presence of Li-bearing micas in G2 (6% muscovite and 2% lepidolite) coupled with the higher modal presence of Fe-bearing minerals (approximately 2%) resulted in the higher Li deportment and lower Li content in the sunken product.

To reduce Fe and Ca contaminants in the sunken products, further magnetic separations should be performed to remove the iron oxides, epidote, and amphibole in the magnetic fraction.

Studies involving the concentration of lepidolite from gangue minerals similar to those observed in this study (muscovite, quartz, and feldspar) were reported using flotation [37]. Commercial lepidolite deposits contain Li in the range of 3.0–4.1 wt% $Li_2O$, some of which can be found in Brazil, Canada, Namibia, Portugal, and Zimbabwe [19].

## 4. Conclusions

In this study, the spodumene liberation, locking, and deportment characteristics of Li-enriched pegmatite samples were assessed through a combination of mineral separation techniques, SEM-based automated mineralogy, and others. This approach helped identify and understand the effect of Li deportment differences on the processing behavior of the samples.

The samples exhibited similar chemical and mineralogical compositions, but different heavy liquid test results. Although having a higher bulk $Li_2O$ content (1.26 wt%) and a higher modal spodumene content (13%), G1 has a lower Li deportment in the sunken product in the heavy liquid test (44%). As both samples presented a high degree of spodumene liberation (approximately 88%), the deportment results were not influenced by the degree of liberation. In fact, Li-bearing mica played a major role in the heavy liquid Li deportment results. Hence, quantifying its Li content was the key to understanding the differences in Li deportment in the heavy liquid test.

The high concentrations of Li and Rb in lepidolite minerals could make them a resource for these elements. Further processing would be necessary to separate them from gangue minerals such as muscovite, quartz, and plagioclase.

Further work is needed to assess the fine size fraction (–0.037 mm) in terms of mineral content, Li deportment, and processing route options. The floated and sunken density separation products from G1 require specific processing routes to recover Li from micas and spodumene, respectively.

**Author Contributions:** Conceptualization, M.T. and C.U.; methodology, M.T. and R.C.; investigation, M.T. and R.C.; resources, C.U.; data curation, M.T.; writing—original draft preparation, M.T.; writing—review and editing, C.U.; supervision, C.U.; project administration, M.T. and C.U.; funding acquisition, C.U. All authors have read and agreed to the published version of the manuscript.

**Funding:** This study was supported by the National Council for Scientific and Technological Development (CNPq), Brazil, Process 437854/2018-3 and 313772/2019-3. Infrastructure was provided by LCT Laboratory. Scholarship from M.T. was provided by Coordination for the Improvement of Higher Education Personnel (CAPES).

**Data Availability Statement:** Data supporting the findings of this study will be made available from the corresponding author, upon reasonable request.

**Acknowledgments:** The authors acknowledge the Technological Characterization Laboratory (LCT-USP) from University of São Paulo for the infrastructure and NAP Geoanalítica-USP (University of São Paulo, Geosciences Institute, Geoanalytical Research Support Center) for the LA–ICPMS instrumentation and support and CAPES for scholarship and CNPq for infrastructure.

**Conflicts of Interest:** The authors declare no conflict of interests.

## References

1. Kavanagh, L.; Keohane, J.; Cabellos, G.G.; Lloyd, A.; Cleary, J. Global Lithium Sources-Industrial Use and Future in the Electric Vehicle Industry: A Review. *Resources* **2018**, *7*, 57. [CrossRef]
2. Martin, G.; Rentsch, L.; Höck, M.; Bertau, M. Lithium Market Research—Global Supply, Future Demand and Price Development. *Energy Storage Mater.* **2017**, *6*, 171–179. [CrossRef]
3. Paes, V.J.C.; Santos, L.D.; Tedeschi, M.F.; Betiollo, L.M. *Avaliação do Potencial do Lítio no Brasil: Área do Médio rio Jequitinhonha, Nordeste de Minas Gerais*; CPRM: Belo Horizonte, Brazil, 2016; ISBN 978-85-7499-283-9.
4. London, D. Ore-Forming Processes within Granitic Pegmatites. *Ore Geol. Rev.* **2018**, *101*, 349–383. [CrossRef]
5. Cerny, P.; Ercit, T.S. The Classification of Granitic Pegmatites Revisited. *Can. Mineral.* **2005**, *43*, 2005–2026. [CrossRef]
6. Ober, A.J. 1994 Minerals Yearbook: Lithium. Available online: https://www.usgs.gov/centers/national-minerals-information-center/lithium-statistics-and-information (accessed on 3 September 2022).
7. Bulatovic, S.M. Beneficiation of Lithium Ores. In *Handbook of Flotation Reagents: Chemistry, Theory and Practice*; Elsevier B.V.: Peterborough, UK, 2014; pp. 41–56. ISBN 9780444530837.
8. Tadesse, B.; Makuei, F.; Albijanic, B.; Dyer, L. The Beneficiation of Lithium Minerals from Hard Rock Ores: A Review. *Min. Eng.* **2019**, *131*, 170–184. [CrossRef]
9. Bale, M.D.; May, A.V. Processing of Ores to Produce Tantalum and Lithium. *Min. Eng.* **1989**, *2*, 299–320. [CrossRef]
10. Evans, K. Lithium. In *Critical Metals Handbook*; John Wiley & Sons, Ltd.: Hoboken, NJ, USA, 2014; ISBN 9781118755341.
11. CBL Produção de Compostos de Lítio No Brasil. Available online: https://www.cetem.gov.br/images/eventos/2016/ii_litio_brasil/apresentacoes/6-producao_de_compostos_de_litio_br.pdf (accessed on 8 June 2020).
12. AMG Lithium Project Update. Available online: https://amg-nv.com/wp-content/uploads/AMG-Lithium-FINAL.pdf (accessed on 10 June 2020).
13. Brandt, F.; Haus, R. New Concepts for Lithium Minerals Processing. *Min. Eng.* **2010**, *23*, 659–661. [CrossRef]
14. Choubey, P.K.; Kim, M.S.; Srivastava, R.R.; Lee, J.C.; Lee, J.Y. Advance Review on the Exploitation of the Prominent Energy-Storage Element: Lithium. Part I: From Mineral and Brine Resources. *Min. Eng.* **2016**, *89*, 119–137. [CrossRef]
15. Oliazadeh, M.; Aghamirian, M.; Ali, S.; Legault, E.; Gibson, C. Flowsheet Development for Benefication of Lithium Minerals from Hard Rock Deposits. In *Global Conference on Extractive Metallurgy the Minerals, Metals & Materials Series*; Springer International Publishing: Pittsburgh, PA, USA, 2018; pp. 2293–2307.
16. Gibson, C.; Aghamirian, M.; Grammatikopoulos, T. The Beneficiation of Lithium Minerals from Hard Rock Deposits. *Min Eng.* **2017**, *69*, 18–37.
17. Jaskula, B.W. 2015 Minerals Yearbook: Lithium. Available online: https://minerals.usgs.gov/minerals/pubs/commodity/lithium/myb1-2015-lithi.pdf (accessed on 25 February 2021).
18. Albermale SC7-2 ALBEMARLE. Available online: https://www.albemarle.com/products/spodumene-concentrate-sc-72-premium (accessed on 20 January 2023).
19. Garrett, D.E. *Handbook of Lithium and Natural Calcium Chloride Uses and Properties*; Elsevier B.V.: Peterborough, UK, 2004.
20. Tran, T.; Luong, V.T. Lithium Production Processes. In *Lithium Process Chemistry*; Elsevier Inc.: Gwangju, Korea, 2015; pp. 81–124. ISBN 9780128014172.
21. Rebouças, L.B.; Souza, M.T.; Raupp-Pereira, F.; Novaes De Oliveira, A.P. Characterization of $Li_2O$-$Al_2O_3$-$SiO_2$ Glass-Ceramics Produced from a Brazilian Spodumene Concentrate. *Ceramica* **2019**, *65*, 366–377. [CrossRef]
22. Aylmore, M.G. Assessment of Lithium Pegmatite Ore Bodies to Determine Their Amenability to Processing for the Extraction of Lithium. In *Global Conference on Extractive Metallurgy the Minerals, Metals & Materials Series*; Springer: Cham, Switzerland, 2018; pp. 2261–2279.

23. Sweetapple, M.T.; Tassios, S. Laser-Induced Breakdown Spectroscopy (LIBS) as a Tool for in Situ Mapping and Textural Interpretation of Lithium in Pegmatite Minerals. *Am. Mineral.* **2015**, *100*, 2141–2151. [CrossRef]
24. Grammatikopoulos, T.; Aghamirian, M.; Fedikow, M.; Mayo, T. Mineralogical Characterization and Preliminary Beneficiation of the Zoro Lithium Project, Manitoba, Canada. *Min. Met. Explor.* **2021**, *38*, 329–346. [CrossRef]
25. Aylmore, M.G.; Merigot, K.; Quadir, Z.; Rickard, W.D.A.; Evans, N.J.; McDonald, B.J.; Catovic, E.; Spitalny, P. Applications of Advanced Analytical and Mass Spectrometry Techniques to the Characterisation of Micaceous Lithium-Bearing Ores. *Min. Eng.* **2018**, *116*, 182–195. [CrossRef]
26. Aylmore, M.G.; Merigot, K.; Rickard, W.D.A.; Evans, N.J.; McDonald, B.J.; Catovic, E.; Spitalny, P. Assessment of a Spodumene Ore by Advanced Analytical and Mass Spectrometry Techniques to Determine Its Amenability to Processing for the Extraction of Lithium. *Min. Eng.* **2018**, *119*, 137–148. [CrossRef]
27. Sandmann, D.; Gutzmer, J. Use of Mineral Liberation Analysis (MLA) in the Characterization of Lithium-Bearing Micas. *J. Miner. Mater. Charact. Eng.* **2013**, *1*, 285–292. [CrossRef]
28. Nascimento, L.S.; Neumann, R.; Ávila, C.A. Mineralogia do Pegmatito da Volta Grande, Região de Nazareno, Minas Gerais: Resultados Preliminares e Inclusões Minerais em Minerais Pesados. In Proceedings of the XXIII—Jornada de Iniciação Cientifica CETEM, Rio de Janeiro, Brazil, 17–21 October 2016.
29. Leißner, T.; Bachmann, K.; Gutzmer, J.; Peuker, U.A. MLA-Based Partition Curves for Magnetic Separation. *Min. Eng.* **2016**, *94*, 94–103. [CrossRef]
30. Wikedzi, A. Comminution Characteristics of Lithium Bearing Mica Ores From Different Devices. *Tanzan. J. Eng. Technol.* **2020**, *39*, 21–31. [CrossRef]
31. Fandrich, R.; Gu, Y.; Burrows, D.; Moeller, K. Modern SEM-Based Mineral Liberation Analysis. *Int. J. Min. Process* **2007**, *84*, 310–320. [CrossRef]
32. Brown, T.; Walter, A.; Idoine, N.; Gunn, G.; Shaw, R.A.; Rayner, D. Mineral Profile: Lithium. Available online: https://www2.bgs.ac.uk/mineralsuk/download/mineralProfiles/lithium_profile.pdf?_ga=2.71957466.851626622.1677422301-1961346163.1677422282 (accessed on 25 February 2021).
33. Munson, G.A.; Clarke, F.F. Heavy-Media Separation Plant and Mine Area Mining and Concentrating Spodumene In the Black Hills, South Dakota. *Min. Eng.* **1955**, *202*, 1041–1045.
34. McIvor, R.E.; Finch, J.A. A Guide to Interfacing of Plant Grinding and Flotation Operations. *Min. Eng.* **1991**, *4*, 9–23. [CrossRef]
35. Gottlieb, P.; Wilkie, G.; Sutherland, D.; Ho-Tun, E.; Suthers, S.; Perera, K.; Jenkins, B.; Spencer, S.; Butcher, A.; Rayner, J. Using Quantitative Electron Microscopy for Process Mineralogy Applications. *JOM* **2000**, *52*, 24–25. [CrossRef]
36. Foster, M.D. Interpretation of the Composition of Lithium Micas. *Geol. Surv. Prof. Pap.* **1960**, *354*, 115–146.
37. Choi, J.; Kim, W.; Chae, W.; Kim, S.B.; Kim, H. Electrostatically Controlled Enrichment of Lepidolite via Flotation. *Mater. Trans.* **2012**, *53*, 2191–2194. [CrossRef]